Supporting Information

Linking Isotope Exchange with Fe(II)-Catalyzed Dissolution of Iron(hydr)oxides in the Presence of the Bacterial Siderophore Desferrioxamine-B

Jagannath Biswakarma[1,2], Kyounglim Kang[3], Walter D.C. Schenkeveld[3†], Stephan M. Kraemer[3], Janet G. Hering[1,2,4] and Stephan J. Hug[1]*

[1]Eawag, Swiss Federal Institute of Aquatic Science and Technology, CH-8600 Dübendorf, Switzerland

[2] Swiss Federal Institute of Technology (ETH) Zurich, IBP, CH-8092 Zürich, Switzerland

[3] University of Vienna, Dept. of Environmental Geosciences, 1090 Vienna, Austria

[4] Swiss Federal Institute of Technology Lausanne (EPFL), ENAC, CH-1015 Lausanne, Switzerland

[*] Corresponding author. E-mail: stephan.hug@eawag.ch

[†] Current address: Copernicus Institute of Sustainable Development, Faculty of Geosciences, Utrecht University, Princetonlaan 8A, 3584 CB, Utrecht, the Netherlands.

Number of pages: 14

Number of tables: 3

Number of figures: 9

Table S1. List of chemicals used for the current study

Chemical Name	**Chemical formale**	**Supplier**	**Purity**	**Stock solution (mM)**
Sodium Chloride	NaCl	Merck	>99%	10
Iron(II) Chloride	$FeCl_2.4H_2O$	Sigma-Aldrich	>99%	10
Iron(III) Chloride	$FeCl_3.6H_2O$	Sigma-Aldrich	>98%	10
Iron (^{57}Fe- 95 atom %, ^{54}Fe 0.04 %, ^{56}Fe 3.04 %, ^{58}Fe 1.86 %)	^{57}Fe	Sigma-Aldrich	≥99.9%	20
Iron -10,000 µg/ml	Fe	J.T Baker	ICP-MS standard	
Desferrioxamine mesylate salt	$C_{25}H_{48}N_6O_8.CH_4O_3S$	Sigma-Aldrich	>92.5%	100
MES (2-morpholino-ethane sulfonic acid monohydrate)	$C_6H_{13}NO_4S.H_2O$	Fluka	>99%	100
MOPS (3-(N-) morpholino propane sulfonic acid)	$C_7H_{15}NO_4S$	Sigma-Aldrich	>99%	100
PIPES (Piperazine-1,4-bis(2-ethane sulfonic acid))	$C_8H_{18}N_2O_6S_2$	Sigma-Aldrich	>99%	100
Sodium (bi)carbonate	$NaHCO_3$	Sigma-Aldrich	>99%	3
o-Phenanthroline	$C_{12}H_8N_2.H_2O$	Fluka	>99%	10

Table S2. List of experiments and experimental conditions. The initial concentration of lepidocrocite or goethite was 1125 µM. (To read the table below: column "Experiments" = first reactant + second reactant; the first reactant was added 1800 s before the second reactant)

Nr.	Experiments[(a)]	Buffers (/pH)
1	20 µM DFOB	Carbonate at pH 7.0 (3 mM $NaHCO_3$, $p(CO_2)$= 0.02 atm)
2	20 µM DFOB + 1 µM Fe(II)	
3	20 µM DFOB + 2 µM Fe(II)	
4	20 µM DFOB + 5 µM Fe(II)	
5	50 µM DFOB	
6	50 µM DFOB + 1 µM Fe(II)	
7	50 µM DFOB + 2 µM Fe(II)	
8	50 µM DFOB + 5 µM Fe(II)	
9	20 µM DFOB + 2 µM ^{57}Fe(II)	Carbonate at pH 7.0 (3 mM $NaHCO_3$, $p(CO_2)$= 0.02 atm)
10	2 µM ^{57}Fe(II) + 20 µM DFOB	
11	50 µM DFOB + 2.2 µM ^{57}Fe(II)	
12	2 µM ^{57}Fe(II) + 50 µM DFOB	
13	2 µM ^{57}Fe(II) + 50 µM DFOB	MES (5 mM) (pH 6.0)
14	50 µM DFOB + 2 µM ^{57}Fe(II)	MOPS (5 mM) (pH 7.0)
15	2 µM ^{57}Fe(II) + 50 µM DFOB	
16	50 µM DFOB + 2 µM ^{57}Fe(II)	PIPES (5 mM) (pH 8.5)
17	2 µM ^{57}Fe(II) + 50 µM DFOB	
18[γ]	2 µM ^{57}Fe(II) + 50 µM DFOB	Carbonate at pH 7.0 (3 mM $NaHCO_3$, $p(CO_2)$= 0.02 atm)
19	2 µM ^{57}Fe(II) + 100 µM phenanthroline	
20[γ]	2 µM ^{57}Fe(II) + 100 µM phenanthroline	

[(a)] Exp. Nr. 1-17 and 20 were conducted with lepidocrocite (Lp).

Exp. Nr. 1-8 were conducted once to examine the effect of added Fe(II) in carbonate-buffered suspensions.

Exp. Nr. 9-18 were conducted (in duplicate) to study the isotope exchange and dissolution.

Exp. Nr. 19-20 were conducted (in duplicate) to assess the isotopic exchange at pH 7.0 without dissolution.

[γ] Experiments were conducted with goethite.

Table S3. Kinetic model with list of complete reactions [(a)]

Nr.	Reaction			Description	K/ *k* pH 7	K/ *k* pH 6
R1	≡Fe^{III} + L	⇄	≡Fe^{III}L	Adsorption of ligand L on surface Fe^{III}	*3.0e5*	*3.0e4-3.0e5*
R1b	≡$^{57}Fe^{III}$ + L	⇄	≡$^{57}Fe^{III}$L	Adsorption of ligand L on surface $^{57}Fe^{III}$	*3.0e5*	*3.0e4-3.0e5*
R2	≡Fe^{III}L	→	≡Fe^{III} + Fe^{III}L	Non-catalyzed dissolution	3.5e-5	n.d.
R2b	≡$^{57}Fe^{III}$L	→	≡Fe^{III} + $^{57}Fe^{III}$L	Non-catalyzed dissolution	3.5e-5	n.d.
R3	$^{57}Fe^{II}$ + L	⇄	$^{57}Fe^{II}$L	Dissolved $^{57}Fe^{II}$L complex formation	*5.3e4*	*3.8e2*
R3b	Fe^{II} + L	⇄	Fe^{II}L	Dissolved Fe^{II}L complex formation	*5.3e4*	*3.8e2*
R4-1a	≡Fe^{III} + $^{57}Fe^{II}$L	→	≡ Fe^{II} + $^{57}Fe^{III}$L	ET from $^{57}Fe^{II}$L to surface Fe^{III} and detachment of $^{57}Fe^{III}$L	1.4e2	200-600
R4-1b	≡Fe^{III} + Fe^{II}L	→	≡ Fe^{II} + Fe^{III}L	ET from Fe^{II}L to surface Fe^{III} and detachment of Fe^{III}L	1.4e2	200-600
R4-1c	≡$^{57}Fe^{III}$ + Fe^{II}L	→	≡ $^{57}Fe^{II}$ + Fe^{III}L	ET from Fe^{II}L to surface $^{57}Fe^{III}$ and detachment of Fe^{III}L	1.4e2	200-600
R4-1d	≡$^{57}Fe^{III}$ + $^{57}Fe^{II}$L	→	≡ $^{57}Fe^{II}$ + $^{57}Fe^{III}$L	ET from $^{57}Fe^{II}$L to surface $^{57}Fe^{III}$ and detachment of $^{57}Fe^{III}$L	1.4e2	200-600
R4-2a	≡Fe^{III}L + $^{57}Fe^{II}$	→	≡ Fe^{II} + $^{57}Fe^{III}$L	ET from $^{57}Fe^{II}$ to surface Fe^{III}L and detachment of $^{57}Fe^{III}$L	2.2e4	-
R4-2b	≡Fe^{III}L + Fe^{II}	→	≡ Fe^{II} + Fe^{III}L	ET from Fe^{II} to surface Fe^{III}L and detachment of Fe^{III}L	2.2e4	-
R4-2c	≡$^{57}Fe^{III}$L + Fe^{II}	→	≡$^{57}Fe^{II}$ + Fe^{III}L	ET from Fe^{II} to surface $^{57}Fe^{III}$L and detachment of Fe^{III}L	2.2e4	-
R4-2d	≡$^{57}Fe^{III}$L + $^{57}Fe^{II}$	→	≡$^{57}Fe^{II}$ + $^{57}Fe^{III}$L	ET from $^{57}Fe^{II}$ to surface $^{57}Fe^{III}$L and detachment of $^{57}Fe^{III}$L	2.2e4	-
R5	≡Fe^{III} + $^{57}Fe^{II}$	⇄	≡Fe^{III}-O-$^{57}Fe^{II}$	Adsorption and desorption of $^{57}Fe^{II}$ on surface Fe^{III}	7.2e6	6.3e4
R5b	≡Fe^{III} + Fe^{II}	⇄	≡Fe^{III} -O-Fe^{II}	Adsorption and desorption of Fe^{II} on surface Fe^{III}	7.2e6	6.3e4
R6	≡Fe^{III}-O-$^{57}Fe^{II}$	⇄	≡$^{57}Fe^{III}$-O-Fe^{II}	ET between ^{57}Fe and ^{56}Fe surface sites	k_{ET}>0.1 K=1	k_{ET}>0.1 K=1
R7	≡$^{57}Fe^{III}$ + Fe^{II}	⇄	≡$^{57}Fe^{III}$-O-Fe^{II}	Adsorption and desorption of Fe^{II} on surface $^{57}Fe^{III}$	7.2e6	6.3e4
R7b	≡$^{57}Fe^{III}$ + $^{57}Fe^{II}$	⇄	≡$^{57}Fe^{III}$-O- $^{57}Fe^{II}$	Adsorption and desorption of $^{57}Fe^{II}$ on surface $^{57}Fe^{III}$	7.2e6	6.3e4

R8	$\equiv Fe^{III}\text{-}O\text{-}{}^{57}Fe^{II} + L$	$\rightarrow$	$\equiv Fe^{II} + {}^{57}Fe^{III}L$	Adsorption of L on adsorbed $^{57}Fe^{II}$, ET and detachment	61	<5
R8b	$\equiv Fe^{III}\text{-}O\text{-}Fe^{II} + L$	$\rightarrow$	$\equiv Fe^{II} + Fe^{III}L$	Adsorption of L on adsorbed Fe^{II} , ET and detachment	61	<5
R9	$\equiv {}^{57}Fe^{III}\text{-}O\text{-}Fe^{II} + L$	$\rightarrow$	$\equiv {}^{57}Fe^{II} + Fe^{III}L$	Adsorption of L on adsorbed Fe^{II} , ET and detachment	61	<5
R9b	$\equiv {}^{57}Fe^{III}\text{-}O\text{-}{}^{57}Fe^{II} + L$	$\rightarrow$	$\equiv {}^{57}Fe^{II} + {}^{57}Fe^{III}L$	Adsorption of L on adsorbed $^{57}Fe^{II}$, ET and detachment	61	<5
R10	$\equiv Fe^{II}$ + Bulk	$\rightarrow$	$\equiv Fe^{III}\text{-}O\text{-}Fe^{II}$	Re-formation of surface site with adsorbed Fe^{II}	*1e10*	*1e10*
R11	$\equiv {}^{57}Fe^{II}$ + Bulk	$\rightarrow$	$\equiv Fe^{III}\text{-}O\text{-}{}^{57}Fe^{II}$	Re-formation of surface site with adsorbed $^{57}Fe^{II}$	*1e10*	*1e10*
R12a	$\equiv Fe^{III}\text{-}O\text{-}{}^{57}Fe^{II}$ + phen	$\rightarrow$	$\equiv Fe^{III}$ + $^{57}Fe^{II}$ phen	Desorption of ^{57}Fe with phen	20 (Gt) 120 (Lp)	-
R12b	$\equiv Fe^{III}\text{-}O\text{-}Fe^{II}$ + phen	$\rightarrow$	$\equiv Fe^{III}$ + $^{57}Fe^{II}$ phen	Desorption of Fe with phen	20 (Gt) 120 (Lp)	-
R12c	$\equiv {}^{57}Fe^{III}\text{-}O\text{-}{}^{57}Fe^{II}$ + phen	$\rightarrow$	$\equiv Fe^{III}$ + $^{57}Fe^{II}$ phen	Desorption of ^{57}Fe with phen	20 (Gt) 120 (Lp)	
R12d	$\equiv {}^{57}Fe^{III}\text{-}O\text{-}Fe^{II}$ + phen	$\rightarrow$	$\equiv Fe^{III}$ +Fe^{II} phen	Desorption of Fe with phen	20 (Gt) 120 (Lp)	
				Initial concentration of active surface sites ($[\equiv Fe^{III}]]_0$)	8.5 µM	8.5 µM

[a] The model appears to be complex, but it consists of the minimal number of reactions that are needed to explain the data. The list of reactions is only long because we need to consider four permutations for all reactions between ^{57}Fe and ^{56}Fe isotopes on the surface and in solution. Although more complex models (for example multisite models) could fit the data more completely, the present model can fit our results reasonably well and supports the proposed mechanisms and reactions pathways.

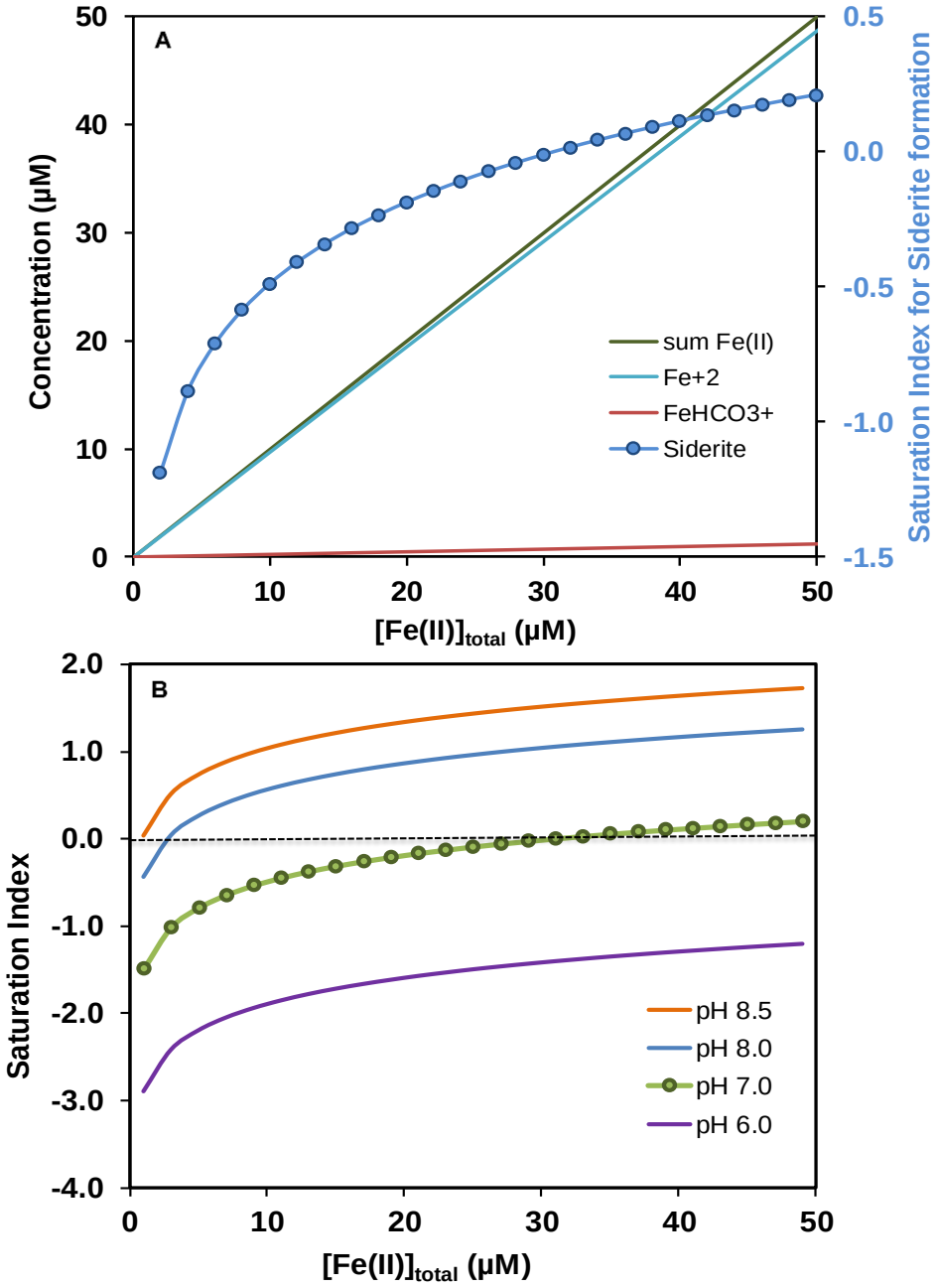

Figure S1. (A) Speciation of Fe(II) with 3 mM $NaHCO_3$ as a function of Fe(II) concentrations at pH 7.0. (B) Saturation index for siderite formation at pH 6, 7.0 , 8.0 and 8.5 in solutions with 3mM $NaHCO_3$. At pH 7.0, solutions are not oversatured with respect to $FeCO_3$ up to concentrations 32 µM Fe(II). Our suspensions with 2 µM and 5 µM are thus far from saturation with $FeCO_3$.

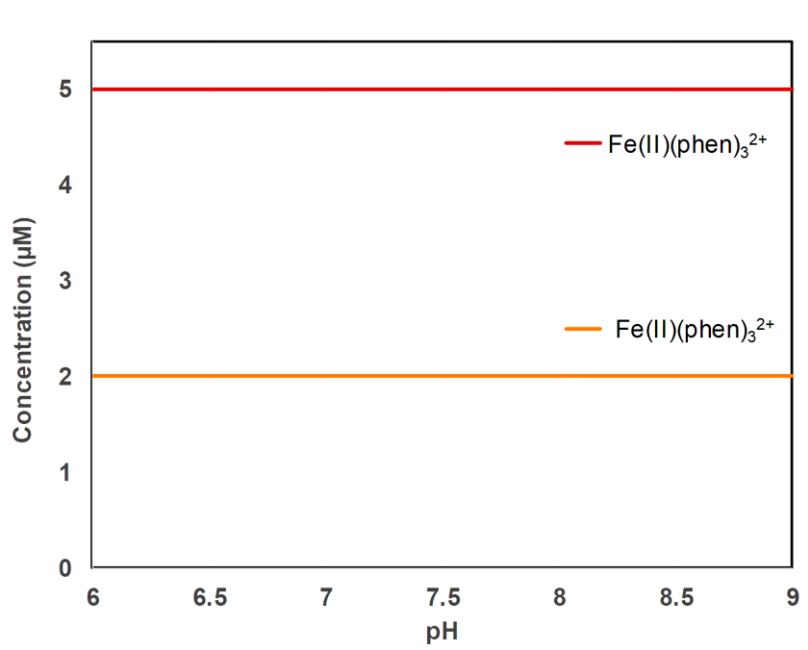

Figure S2. Calculated speciation of 2 µM (orange line) and 5 µM Fe(II) (red line) in a solution with 3 mM Na^+, 3 mM alkalinity and 100 µM phen. The only species with concentrations above 1 nM are $Fe(II)(phen)_3^{2+}$.

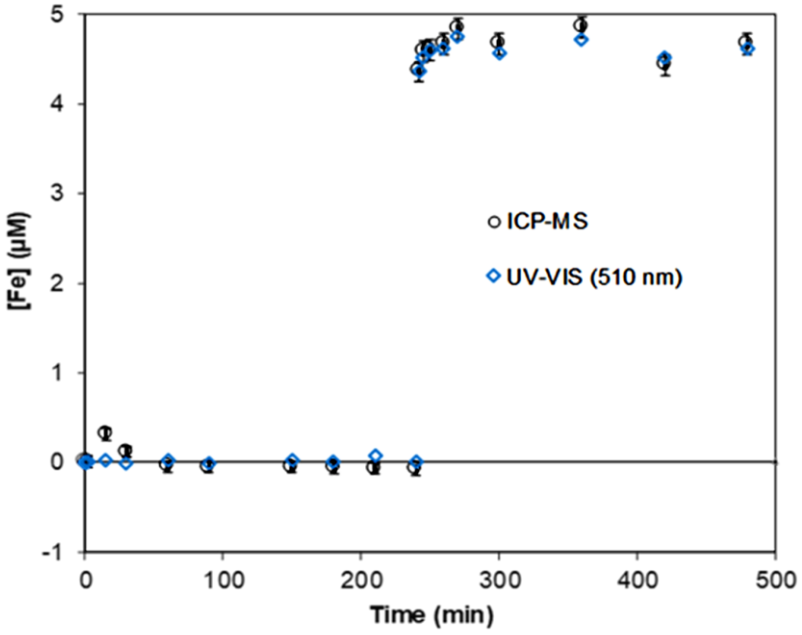

Figure S3. Dissolved total Fe and Fe(II) in filtered samples of a 1.13 mM Lp suspension with 100 µM phen in 3 mM $NaHCO_3$ at pH 7.0 (anoxic). No Fe was added for the first 240 min. At 245 min, 5 µM Fe(II) was added. $Fe(II)(phen)_3^{2+}$ was quantified with UV-Vis at 510 nm (ε=11'000 $M^{-1}cm^{-1}$). Total dissolved Fe was measured with ICP-MS. Phen alone caused no dissolution (detection limit ±0.1 µM). Added Fe(II) led to formation of $[Fe(II)(phen)]_3^{2+}$ at the expected concentration, which shows that $[Fe(II)(phen)]_3^{2+}$ does not, or only very weakly, adsorb to the surface.

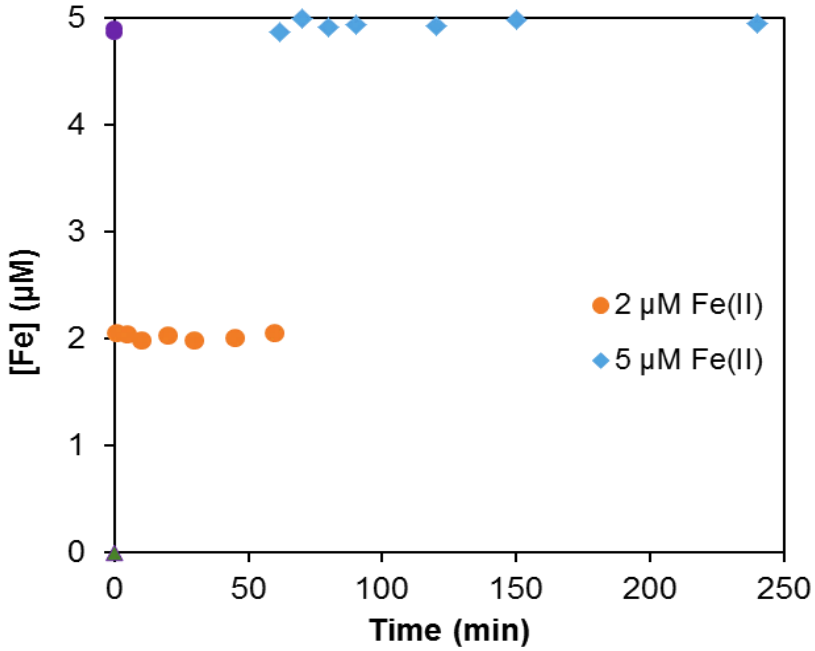

Figure S4. Control experiment with 1.13 mM Lp and100 µM phen in 3 mM $NaHCO_3$ at pH 7.0. 2 µM Fe(II) was added at 0 min (orange circles), followed by addition of 3 µM Fe(II) after 60 min to a total concentration of Fe(II) of 5 µM (blue diamonds). The concentration of the $Fe(II)(phen)_3^{2+-}$ was measured with UV-VIS at 510 nm. The green triangle at 0 min shows the blank with no added Fe(II) and the purple circle the concentration of $Fe(II)(phen)_3^{2+}$ with 5 µM Fe(II) without Lp. The experiment confirms that less than of 5% of $Fe(II)(phen)_3^{2+}$ was adsorbed at both concentrations.

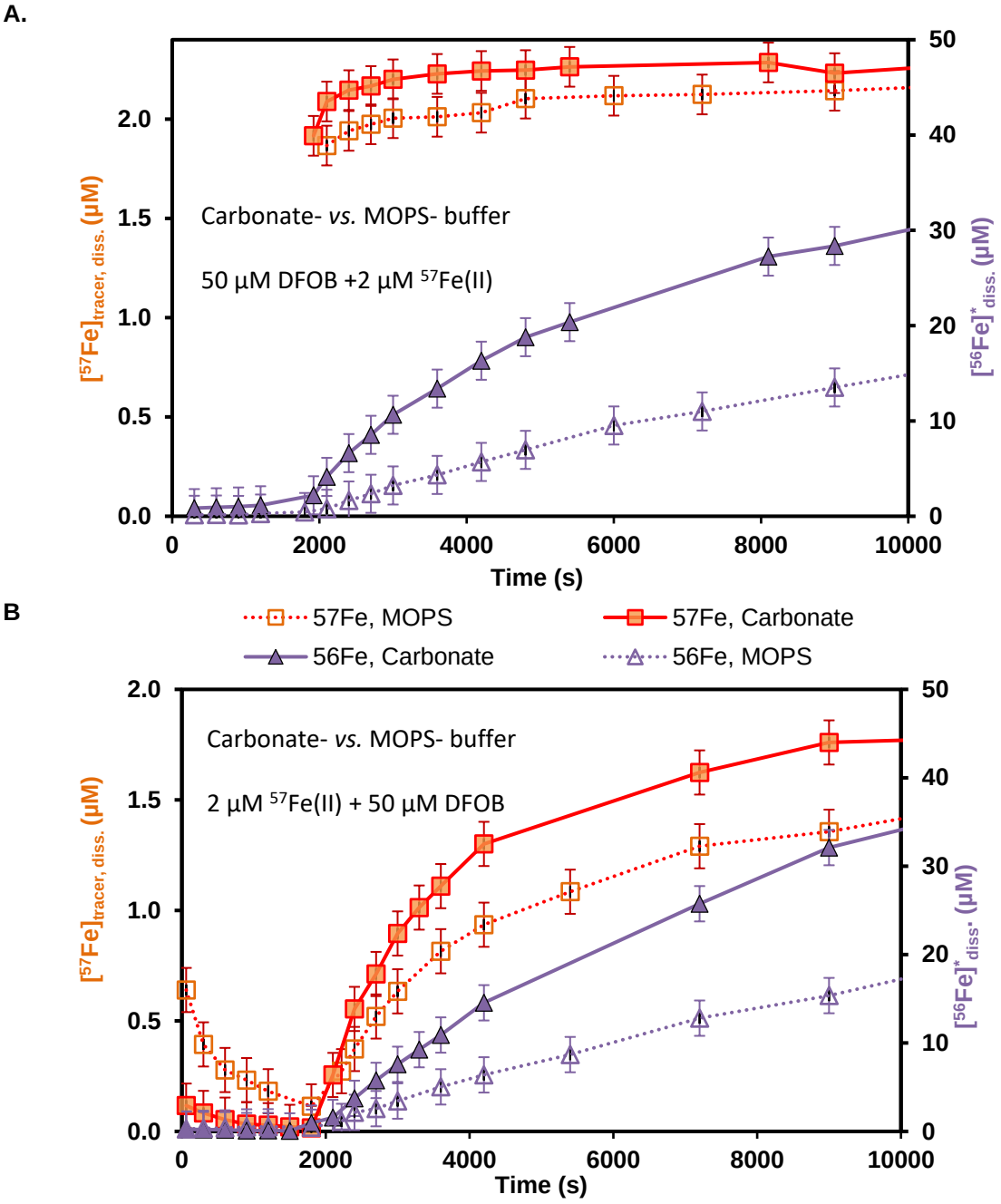

Figure S5. Comparison of carbonated-buffered (filled symbols) and MOPS-buffered (empty symbol) systems (pH 7.0); anoxic conditions. (A) 2 µM ^{57}Fe(II) was added 1800 s after 50 µM DFOB addition. (B) 2 µM ^{57}Fe(II) was added 1800 s before 50 µM DFOB addition. Error bars correspond to the standard deviations of ICP-MS measurements obtained from repeated calibrations. Lines are to guide eyes through the data points. Symbols: triangles (right axis): concentration of Fe released into solution by Lp dissolution ($[^{56}Fe]^*_{diss.}$); squares (left axis): dissolved concentration of tracer ^{57}Fe corrected for the natural abundance of ^{57}Fe in Lp ($[^{57}Fe]_{tracer, diss.}$).

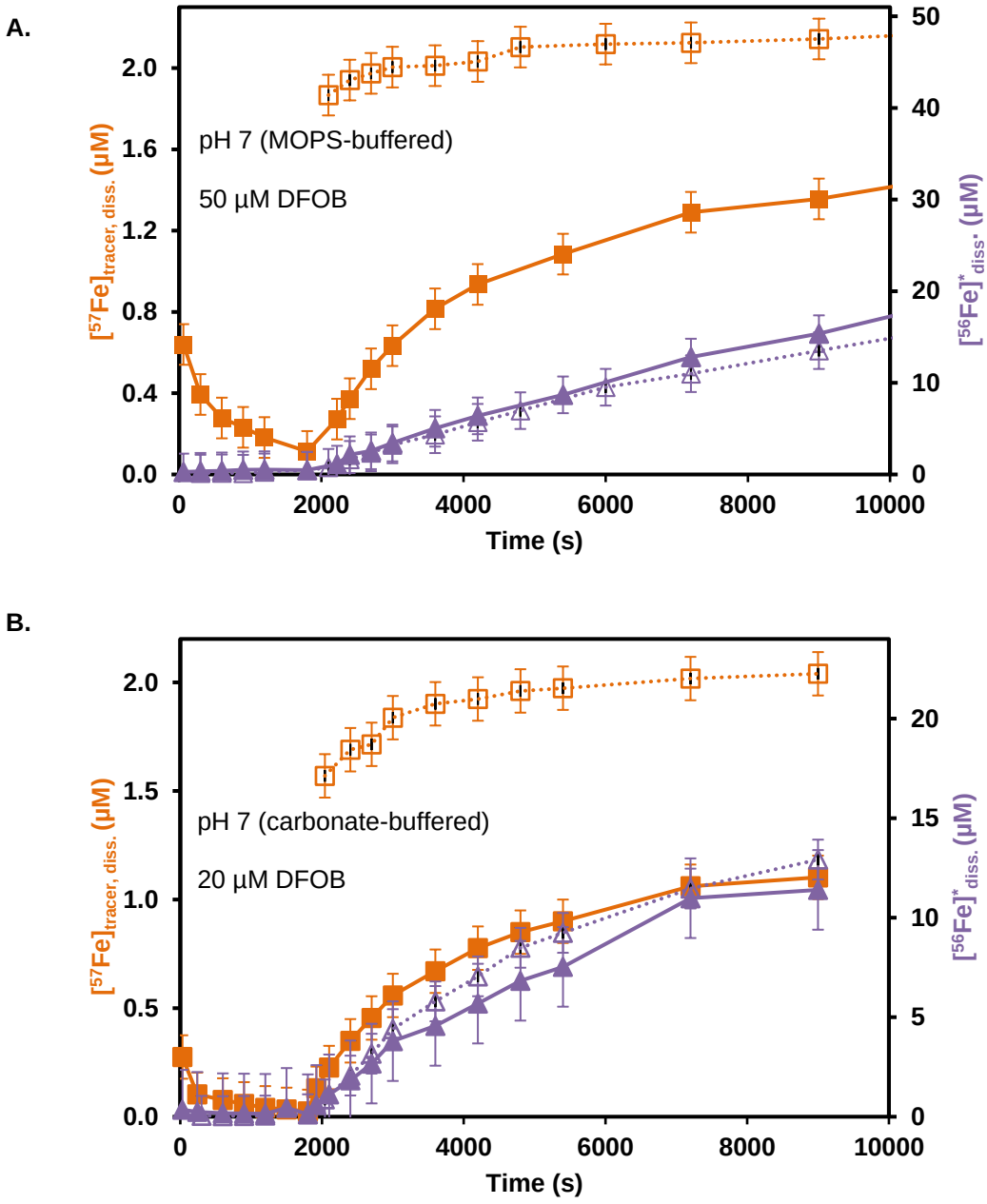

Figure S6. ^{57}Fe isotope exchange and Lp dissolution as a function of time (A) with 50 µM DFOB at pH 7.0 (MOPS- buffered), and (B) with 20 µM DFOB at pH 7 (carbonate-buffered). 2 µM ^{57}Fe(II) was added to a Lp suspension (1125 µM) 1800 s before (filled symbols) or after (empty symbols) DFOB addition under anoxic conditions. Error bars correspond to the standard deviations of ICP-MS measurements obtained from repeated calibrations. Lines serve as visual guide. The data for ^{57}Fe (filled squares) and ^{56}Fe (filled triangles) after 1800 s are also shown in main Figure 3.

Symbols: (purple) triangles (right axis): concentration of Fe released into solution by Lp dissolution ($[^{56}Fe]^*_{diss.}$); (orange) squares (left axis): dissolved concentration of tracer ^{57}Fe corrected for the natural abundance of ^{57}Fe in Lp ($[^{57}Fe]_{tracer, diss.}$).

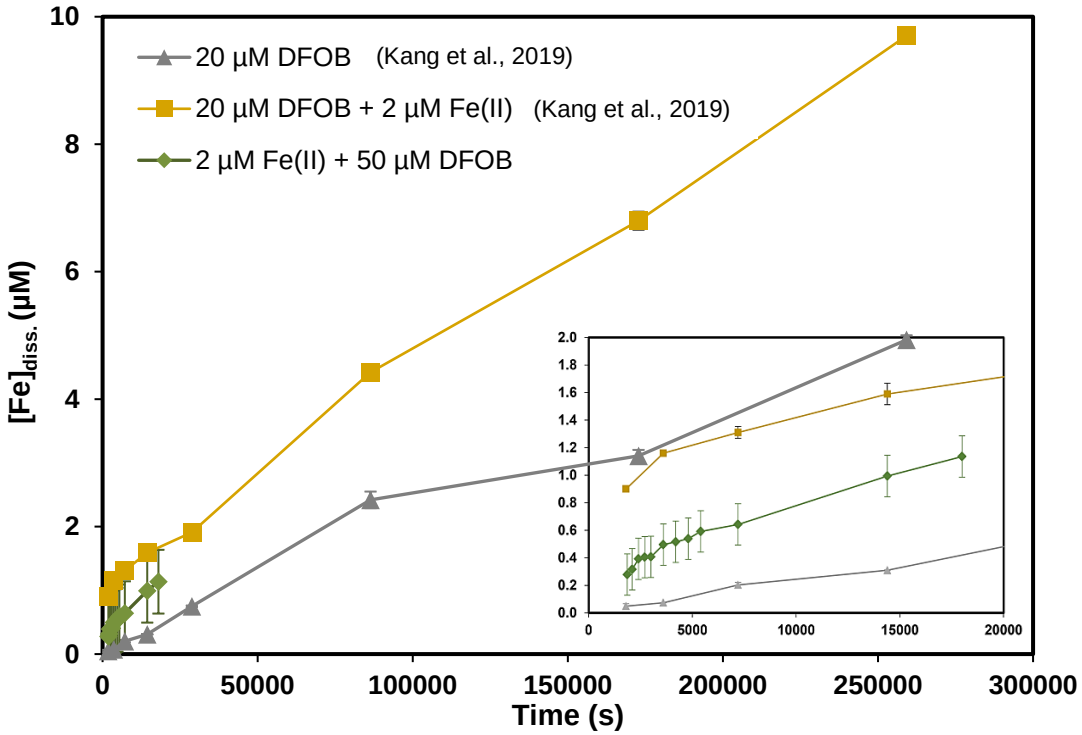

Figure S7. Goethite dissolution at pH 7 under anoxic condition. ^{57}Fe(II) was added , as a tracer for Fe(II), 1800 s before DFOB (50 µM) to a goethite suspension (1125 µM) in carbonate-buffered system. Experiments were conducted in duplicates (n=2). Note that Kang et al., 2019[1] conducted goethite dissolution experiments in MOPS-buffered conditions by adding both DFOB and Fe(II) at a same time. The inset figure is to highlight the first 20 000 s measurements. Lines serve as visual guides.

Goethite dissolution is slower than Lp dissolution (Kang et al. 2019). Our results show that only 1.14 µM goethite dissolution was measured after 5 hr. (20 000 s), when ^{57} Fe(II) was added 1800 s before 50 µM DFOB. When compared to measurements by Kang et al., goethite dissolution within the same time frame was found almost in agreement. Although the concentration of dissolved Fe was measured as 1.57 µM by Kang et al., the differences in measurments could be due to the difference in the applied DFOB concentrations and to the reversed addition of Fe(II). Currently we lack data to explain these subtle differences. However, the key purpose of applying ^{57}Fe(II) before DFOB was to examine the release of ^{57}Fe during accelerated goethite dissolution (as shown by Figure 4).

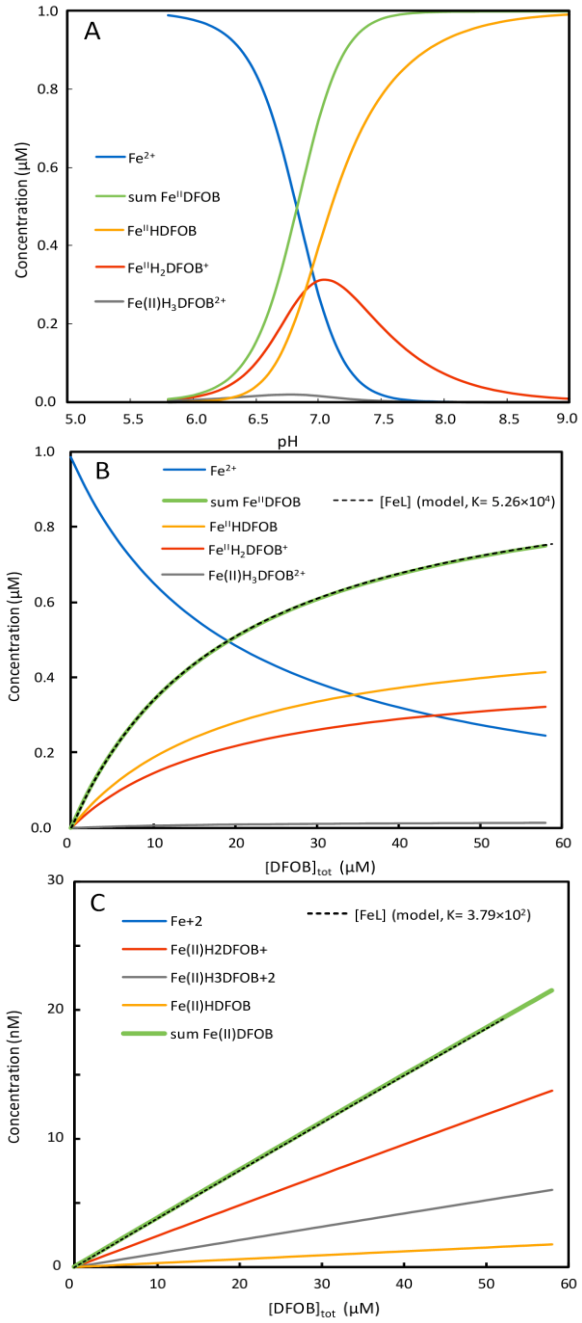

Figure S8. A: Speciation of 1 µM Fe(II) with 50 µM DFOB, 3 mM Na^+ and 3 mM HCO_3^- as a function of pH. B and C: Speciation of 1 µM Fe(II) as a function of total DFOB (1-60 µM), 3 mM Na^+ and 3 mM HCO_3^- at pH 7.0 (B) and pH 6.0 (C). The speciation was calculated with Visual MINTEQ Ver, 3.1 (Jon Petter Gustafsson, KTH, SEED, Stockholm, Sweden) with complexation constants for DFOB and Fe(II) (from Kim et al., 2010[2]) added to the Visual MINTEQ database. In the kinetic model (Table 1), conditional complex formation constants for the formation of $Fe^{II}L$ (sum of Fe(II)HDFOB, $Fe(II)H_2DFOB^+$ and $Fe(II)H_3DFOB^{2+}$) at pH 7 and pH 6 were used. The conditional complex formation constants were obtained by the values for K_L which provide the best fits of $[Fe^{II}L] = [Fe^{II}]_o(K_L*[L]/(1+K_L*[L]))$ to the output of Visual MINTEQ (thin dashed black lines, Figures B and C).

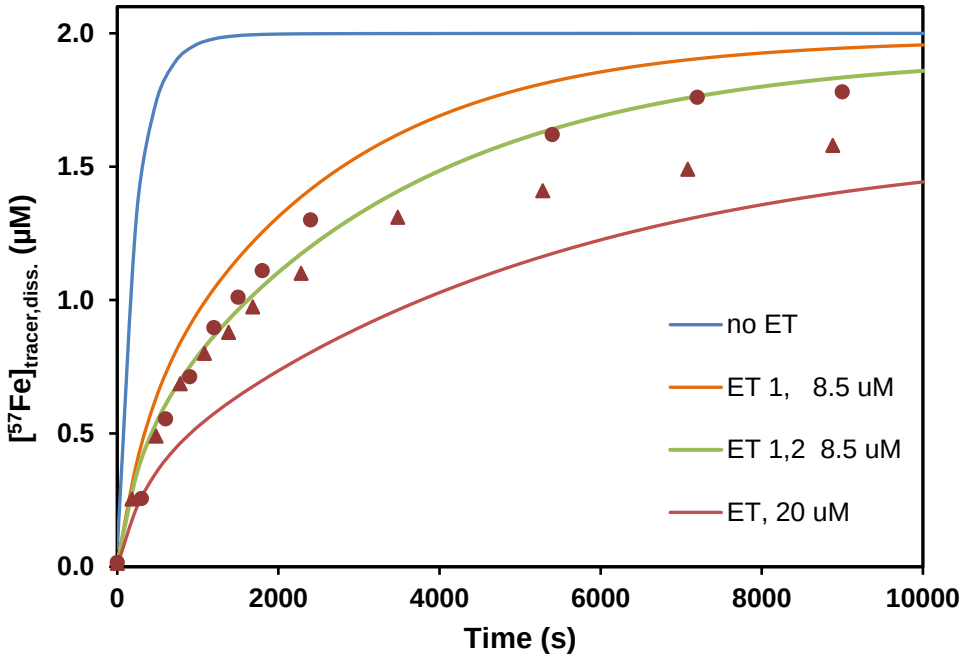

Figure S9. Modeled and measured release of ^{57}Fe after addition of 50 µM DFOB to Lp (1.13 mM) with 2 µM adsorbed ^{57}Fe(II). Without ET during adsorption and dissolution (blue line), the model predicts a very quick release of adsorbed ^{57}Fe(II). With ET and distribution of negative charge over 8.5 µM surface sites only during adsorption (orange line; ET 1), the predicted release is slower, but still faster than observed experimentally. With ET and distribution of charge over 8.5 µM surface sites during adsorption and dissolution (green line; ET 1, 2), the model matches the observed release of ^{57}Fe, particularly during the first 4000s where the data is more reliable. (At later times, dissolution rates can slow down due to oxidation of Fe(II) by residual oxygen). With distribution of charge over more surface sites, for example 20 µM (red line), the predicted release of ^{57}Fe is slower than observed.

References

1. Kang, K.; Schenkeveld, W. D. C.; Biswakarma, J.; Borowski, S. C.; Hug, S. J.; Hering, J. G.; Kraemer, S. M., Low Fe(II) Concentrations Catalyze the Dissolution of Various Fe(III) (hydr)oxide Minerals in the Presence of Diverse Ligands and over a Broad pH Range. *Environ. Sci. Technol.* **2019,** *53*, (1), 98-107.
2. Kim, D.; Duckworth, O. W.; Strathmann, T. J., Reactions of aqueous iron-DFOB (desferrioxamine B) complexes with flavin mononucleotide in the absence of strong iron(II) chelators. *Geochim. Cosmochim. Acta* **2010,** *74*, (5), 1513-1529.